Heliyon 7 (2021) e06684

Contents lists available at ScienceDirect

Heliyon

journal homepage: www.cell.com/heliyon

Research article

Binding mechanism of naringenin with monoamine oxidase – B enzyme: QM/MM and molecular dynamics perspective

Hunday Govindasamy, Sivanandam Magudeeswaran, Saravanan Kandasamy, Kumaradhas Poomani *

Laboratory of Biocrystallography and Computational Molecular Biology, Department of Physics, Periyar University, Salem, 636 011, India

ARTICLE INFO

Keywords:
Parkinson's disease
Binding free energy
Monoamine oxidase
Naringenin
Molecular docking
QM/MM
Molecular dynamics

ABSTRACT

The reduced level of dopamine at midbrain (substantia nigra) leads to Parkinson disease by the influence of monoamine oxidation process of monoamine oxidase B (MAO-B) enzyme. This disease mostly affects the aged people. Reports outline that the naringenin molecule acts as an inhibitor of MAO-B enzyme and it potentially prevents the development of PD. To elucidate the binding mechanism of naringenin with MAO-B, we performed the molecular docking, QM/MM and molecular dynamics (MD) simulations. The molecular docking results confirm that the naringenin strongly binds with the substrate binding site of MAO-B enzyme (-12.0 kcal/mol). The low values of RMSD, RMSF and Rg indicate that the naringenin – MAO-B complex is stable over the entire period of MD simulation. Naringenin forms strong interaction with the orient keeper residue Tyr326 and other binding site residues Leu171, Glu206 and these interactions were maintained throughout the MD simulation. It is also important to block the function of MAO-B enzyme. The QM/MM study coupled with the charge density analysis reveals the charge density distribution and the strength of intermolecular interactions of naringenin-MAO-B complex. The above results suggest that this molecule is a potential inhibitor of MAO-B enzyme.

1. Introduction

In worldwide, the aged people largely facing one of the most familiar brain disorders is Parkinson's disease (PD) [1]. This brain disorder causes a gradual loss of muscle movement and control. Reportedly, this disease originate in the mid-brain (substantia nigra), where the motor function signaling cells become as the poorly performing cells to send the signal to various parts of the body, which leads to PD and their associated diseases [2, 3]. This is predominantly due to the reduced dopamine substance level at midbrain by the influence of monoamine oxidation process of monoamine oxidase B type (MAO-B) enzyme. The dopamine is metabolite into inactive form by the MAO-B enzyme. These impacts are involved to reduce the level of dopamine (neurotransmitter) known to be monoamine chemical substance, which is required to transfer the signal for the action of organ through the neuron cell [4, 5]. The lower level of dopamine at *substantia nigra* causes PD. MAO-B enzyme is the family of flavin-containing amine oxidoreductase enzyme, which oxidizes the monoamines (adrenaline, noradrenaline, serotonin and dopamine) [6, 7]. The MAO-B enzyme is expressed from MAO-B gene, which appears over the mitochondrial membrane with notable activities in neurons cell (central nervous systems and peripheral tissue). The MAO-B enzyme contains 520 amino acids, a co-factor Flavin adenine dinucleotide (FAD) and substrate dopamine. Apart from this, it has an entrance cavity residue Ile199; this behaves as an open and close type of conformation which allows to enter the substrate (dopamine). After the substrate enters into the binding site, the enzyme catalyzes the amine group of substrate by deamination process. In this reaction, the FAD is converted into FADH2 by the massive responses of Lys296 and water molecule [8, 9]. Subsequently, the tyrosine residues (Tyr326, Tyr398 and Tyr435) keep the orientation of substrate for the Oxidation mechanism. And also, it increases the nucleophilicity of the substrate amine, which leads the amine group into imine group. Notably, without the influence of enzyme, this imine group of substrate undergoes the hydrolysis process and converted into carbonyl group. Thus, the MAO-B enzyme metabolizes the substrates into the inactive forms [10]. Apart from the above said mechanisms, the computational studies by Li and Son et al., outline three catalytic scenarios; such as radical, the polar nucleophilic and direct hydride mechanisms [11, 12]. Whereas, Vianello et al., proposed new two-step catalytic hydride reaction for the degradation of dopamine by Monoamine oxidase enzyme [13]. Further, the studies by Abad et al., confirm

* Corresponding author.
E-mail address: kumaradhas@yahoo.com (K. Poomani).

https://doi.org/10.1016/j.heliyon.2021.e06684
Received 12 October 2020; Received in revised form 31 December 2020; Accepted 30 March 2021

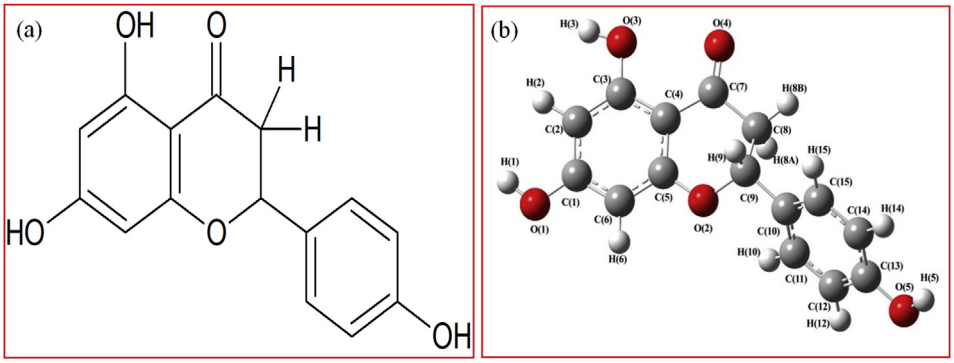

Figure 1. (a) Chemical structure and (b) Optimized structure of naringenin molecule.

the above said polar nucleophilic contribution through QM/MM calculations [14] and Atalay et al., confirms the hydride transfer mechanism is more suitable for the oxidation of dopamine [15]. In this perspective, notably, Zapata et al., observed that the MAO-B enzyme prefers the hydride transfer mechanism [16].

Further, the mutation present in the binding site residues of MAO-A and MAO-B enzymes alters their oxidation reaction. Oanca et al., states that the presents of mutation (I335Y) and large number of water molecules in the binding site of MAO-A enzyme affects the catalytic mechanism [17]. Poberznik et al., found that the catalytic mechanism of both MAO-A and MAO-B occurs via the hydride transfer mechanism, but the mutations of aromatic cage (Tyrosine) residues alters the catalytic mechanism [18]. Pregeljc et al., investigates the effect of point mutation (Y326I) presents in the binding site of MAO-B enzyme. They concluded that, the point mutation and excess of water molecules present in the binding site diminishes the catalytic mechanism [19]. Furthermore, the electrostatic interactions are involved in the primary role of enzymatic mechanism of MAO (A, B) enzymes. Prah et al., elucidated that the electrostatic interaction between MAO-A and Phenylethylamine [9]. Tandaric et al., proposed the irreversible mechanism of MAO-B enzyme using propargylamine inhibitors (Selegiline and Rasagiline) through the rate-limiting hydride abstraction step. The results concluded that, the Selegiline strongly binds with FAD compared with Rasagiline [20, 21].

The dopamine level could increase through the inhibition of MAO-B enzyme and that could prevent the effects of PD. The *in vitro* study is one of the prominent techniques allows to find out the suitable drug molecules to stop the irregular function of enzymes [22, 23, 24]. Recent reports (*in vitro)* outline that the South African traditional medicine extracted from Mentha aquatica, Scotia brachypetala, Ruta graveolens and Gasteria croucheri (naringenin) shows high inhibition rate against MAO-B enzyme [24]. Usually, naringenin (Figure 1a) is found in citrus fruits like grapes, oranges, tomatoes, etc. [25, 26]. It also exhibits several medicinal effects [27], such as on preventing the heart disease [28], hypertension [29], stop promoting of low-density lipoprotein secretion [30], human cancer, tumor activity [31] and hepatitis C [32]. Similarly, it has an inhibitory effect against cytochrome [33] and oxidant agent [34, 35, 36]. The anti-oxidant properties of this molecule helps to control the degradation of dopamine, which inhibits the MAO-B enzyme [37]. Although the *in vitro* and *in silico* studies reveal the naringenin molecule inhibits MAO-B enzyme function [38], the molecular mechanism such as binding mode, conformation and its stability of naringenin is not yet elucidated briefly. The current study is mainly focused to predict the mode of binding through the interactions, conformational modification, stability and the binding energy of naringenin in the binding site of MAO-B enzyme by using molecular docking and molecular dynamics simulations. Since the binding mode is large contribution of intermolecular interactions between the naringenin and MAO-B enzyme, this study explores the geometry and topology of electron density from the quantum mechanical and molecular mechanics (QM/MM) method. Further, the stability of naringenin in the binding site of MAO-B enzyme has been analyzed and the binding energy also determined from the MD simulations.

2. Materials and methods

2.1. Molecular docking analysis

The molecular docking is a tool being used for docking of ligands in the binding site of protein and protein-protein and further to explore the binding nature of the molecules in the complexes. In this *in silico* study, the naringenin molecule is docked in the binding site of MAO-B enzyme and then analyzed. Ligand and protein preparation: initially, the naringenin structure was obtained from Pubchem data base; further the density functional theory performed by using the B3LYP/6-311G** basis set to optimize the naringenin molecule using *GAUSSIAN03* software [39, 40]. Further the *Ligprep* module was used to prepare the naringenin molecule with Optimized Potentials for Liquid Simulations force field (OPLS_2005) [41,42]. The protein molecule was obtained from the Protein Data Bank (PDB ID: 1S3E) of resolution 1.6 Å. To carry out the molecular docking, initially, we removed the water molecules (beyond 5 Å from the binding site) from the MAO-B enzyme. Further using protein preparation *wizard*, the missing residues, common bond orders, charges and the hydrogen atoms were added [41]. The binding site region of MAO-B enzyme was predicted using the *sitemap* application [43]. The molecular docking study of naringenin–MAO-B enzyme explored using Induced Fit Docking (IFD) [44] method using *Schrödinger* programme suite [44, 45]. The detailed intermolecular interactions (hydrogen bonding and hydrophobic) of naringenin-MAO-B complex were analyzed using *PyMol* [46], *Chimera* [47] and *Ligplot* [48] and discussed in detail.

2.2. Molecular dynamics simulation

The Molecular dynamics simulation (MD) analysis reveals the conformational modification and the stability of naringenin when it is present in the binding site of MAO-B enzyme. Initially, the general *AMBER Force Field* was used to prepare [49] the coordinate and topological files of naringenin molecule followed by the *AMBERff14SB* force field [50] used for naringenin-MAO-B complex using *leap* module of *Antechamber* suite [51]. Thus prepared complex was solvated using *TIP3P* water model at the boundary distance of 10 × 10 × 10 Å. To stabilize the charges of the system, the chlorine ions ($9Cl^-$) were added [52, 53]. Then the MD simulation was performed from *AMBERTOOLS14* package [54]. Before the MD simulation, the complex was minimized at 2000 steps in both *steepest descent* (first 500 step) and *conjugate gradient* (remaining 1500 steps) methods; followed by using NVT ensemble, the naringenin-MAO-B complex was annealed from 0 to 300 K at 500 ps [55]. Successively, the equilibration was performed using NPT ensemble at 500 ps with the same *Berendsen barostat* and *Langevin thermostat* used in

Table 1. IFD score (kcal/mol) values of Naringenin molecules with MAO-B enzyme.

Conformers	Docking score	Glide energy	Prime Energy	IFD Score
1	-12.029	-51.074	-21690.8	-1096.57
2	-11.717	-52.121	-21681.7	-1095.81
3	-11.490	-50.296	-21707.3	-1096.86
4	-12.035	-49.749	-21687.7	-1096.42
5	-10.987	-49.531	-21701.8	-1096.08
6	-11.011	-49.151	-21679.2	-1094.97
7	-11.144	-49.024	-21700.1	-1096.15
8	-9.8103	-48.746	-21687.1	-1094.16
9	-11.269	-48.630	-21700.6	-1096.3
10	-11.682	-48.327	-21691.3	-1096.25
Dopamine	-8.044	-28.969	-20851.9	-1050.64

the heating process [56, 57]. The final production process was started for 50 ns at time step of 2 fs with NPT ensemble (constant temperature 300 K and pressure 1.0 tar). Using *SHAKE* algorithm, the bonds of hydrogen atoms (non-polar only) were constrained [58]. The MD simulation trajectories were extracted and analyzed using *CPPTRAJ* module [59]. The final MD trajectories were examined and plotted using *XMgrace and VMD* packages [60, 61]. The MM/GBSA method was consumed to find out the binding free energy of naringenin-MAO-B complex; in which the entropy (TΔS) was not included. The normal mode analysis was used to calculate the entropy contribution in ligand binding and it was included in the free energy calculation [62, 63].

2.3. QM/MM study

The quantum mechanical and molecular mechanics (QM/MM) is a useful tool to predict the electronic level information of binding pocket (ligand-protein interactions) using the combined QM and MM method. The quantum chemical calculation is suitable for very less number of atoms; because, the QM approach of macromolecular system (protein, lipids, polymer, RNA and DNA) is time consuming process and difficult to solve the Schrodinger equations. In the QM/MM calculations, the ligand-protein complex is divided into two regions, such as principal QM and MM regions; in the present study, the QM region exhibits the naringenin molecule which interacts with the nearest binding site amino acids of MAO-B enzyme. The semi-empirical method was used to compute the QM region with PM3 and suitable basis set. Except QM region, the entire complex was treated as molecular mechanics region with a force field using *AMBERTOOLS14*. The QM/MM input files obtained from the MD simulation and the minimization was performed at 2000 cycles; the initial minimization take place in the *steepest descent* method (500 steps), subsequently, remaining 1500 steps were performed using the *conjugate gradient* method with micro-canonical ensemble (NVE) [64]. The QM/MM explores the distribution of electron density in the region of intermolecular interactions between naringenin molecule and the nearest binding site residues of MAO-B enzyme [65]. The topological properties of electron density at the critical point (*cp*) [($\rho_{cp}(r)$ and $\nabla^2\rho_{cp}(r)$] were calculated for the intermolecular interactions (hydrogen bonding interactions) using *AIMPAC* software [66, 67]. using *wfn2plots* and *denprop* from *XD2006* package [68], The deformation and Laplacian of electron density ~~of~~ for intermolecular interactions were mapped.

3. Results and discussion

3.1. Naringenin intermolecular interactions with MAO-B enzyme

The current study aims to elucidate the mode of binding of naringenin molecule into the binding site of the MAO-B enzyme and how it establishes the key contacts with the binding site residues of MAO-B enzyme. This allows to identify the potential ligand to inhibit the MAO-B enzyme as it is necessary to control the dopamine level [69]. The optimized structure of naringenin molecule [Figure 1(b)] was used for the molecular docking to explore the binding mechanism, such as molecular conformation, orientation and the intermolecular interactions of naringenin in the binding site of MAO-B enzyme through induced fit docking (IFD) study [45, 70]. The naringenin molecule was strongly binds with the binding site of MAO-B enzyme which was explored from the IFD analysis. Based on the glide energy (-51.074 kcal/mol), docking score (-12.029 kcal/mol), prime energy (-21690.81 kcal/mol), IFD score (-1096.57 kcal/mol) and the intermolecular interactions, the best conformer (conformer-1) was preferred for further analysis (Table 1) [71, 72, 73, 74]. Figure 2(a-b) displays the intermolecular interaction of naringenin molecule with the binding site residues of MAO-B enzyme.

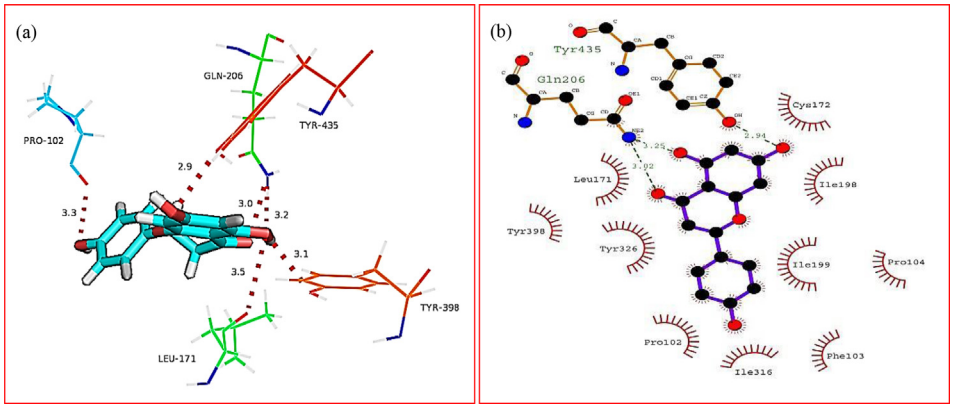

Figure 2. Display the intermolecular interactions of Naringenin-MAO-B complex (a) hydrogen bonding interactions analyzed from *PyMol* and (b) hydrophobic contribution visualized from *ligplot*.

Table 2. The intermolecular interaction distances (Å) of naringenin with binding site residues of MAO-B enzyme.

Binding Site residues	Naringenin atom···amino acid residues and atom identifier	Docking	QM/MM	MD simulation
Pro102	O(5)···Pro102/O	**3.3**	**2.8**	7.0
Pro104	O(5)···Pro104/CD	3.2	3.7	6.6
Phe168	O(5)···Phe168/CA	7.2	7.4	3.5
Leu171	O(1)··· Leu171/O	5.1	5.3	**2.5**
Leu171	O(5)···Leu171/CD1	10.0	10.1	3.6
Leu171	O(3)···Leu171/O	**3.5**	**2.8**	6.3
Cys172	O(1)··· Cys172/SG	3.4	3.5	7.4
Ile198	O(1)···Ile198/CB	3.7	3.7	9.4
Ile199	C(13)···Ile199/CG2	4.3	4.5	3.6
Ile199	C(13)···Ile199/CD1	3.7	4.2	5.9
Gln206	O(4)···Gln206/NE2	**3.0**	**2.9**	5.3
Gln206	O(2)···Gln206/NE2	5.3	5.1	**2.9**
Gln206	O(3)···Gln206/NE2	**3.2**	3.9	6.4
Lys296	O(3)···Lys296/NZ	7.7	9.6	9.0
Ile316	O(5)···Ile316/CG2	3.6	5.9	6.9
Tyr326	O(4)···Tyr326/OH	4.6	4.5	3.9
Tyr326	O(4)···Tyr326/CE1	3.0	3.1	3.0
Phe343	O(3)···Phe343/CD1	5.7	6.3	3.0
Tyr398	O(3)···Tyr398/OH	**3.1**	**3.2**	8.7
Tyr398	O(1)···Tyr398/CD1	8.3	5.8	4.0
Tyr435	O(1)···Tyr435/OH	**2.9**	**2.7**	8.4
FAD502	O(3)···FAD502/O4	8.5	7.8	3.8

The hydrogen bonding interaction distances are shown in bold to differentiate from other interactions.

The interactions between naringenin and the binding site residues of MAO-B enzyme were analyzed, and found that the naringenin molecule is appearing strong interactions with the substrate binding site and gate residues of MAO-B enzyme [75]. The electronegative atom (oxygen) of naringenin molecule forms solid interactions with the binding site residues of MAO-B enzyme (Table 2). Notably, the hydrogen bonding interaction of O(1)···H–O/Tyr435 and O(3)···H–O/Tyr398 formed between orient keeper residues (Tyr435 and Tyr398) of MAO-B enzyme and with the O(1), O(3) atoms of naringenin molecule, the interaction distances are 2.9 and 3.1 Å respectively and these residues are responsible to keep the orientation of naringenin in the binding site of MAO-B enzyme. Similarly, the O(3), O(4) and O(5) oxygen atoms of naringenin molecule also forms hydrogen bonding interactions with the residues Pro102, Leu171, and Gln206 at the distances of 3.3, 3.5, 3.0 and 3.2 Å respectively [O(5)–H(13)···O/Pro102, O(3)–H(3)···O/Leu171, O(4)···H–N/Gln206 and O(3)···H–N/Gln206]. The O(1) atom of naringenin molecule forms nearest amino acids contact with Cys172 and Ile198 at the distances of 3.4 and 3.7 Å; similarly, the O(5) atom also forms interaction with Pro104 (3.2 Å) and Ile316 (3.6 Å) residues. Furthermore, the hydrophobic interaction (3.7 Å) also found between C(13) atom of naringenin and the gate residue (Ile199). The above said interactions between naringenin and MAO-B enzyme confirms that the naringenin molecule potentially interacts with the MAO-B enzyme.

3.2. Topological properties of electron density of intermolecular interactions

The QM/MM analysis has been achieved to explicit the onsite studies of interaction between naringenin and MAO-B enzyme. It shows that the O(1), O(2), O(3), O(4) and O(5) oxygen atoms of naringenin molecule forms interaction with the binding site residues of MAO-B enzyme as predicted ~~in~~ from molecular docking study (Table 2). Notably, in molecular docking the O(1), O(3), O(4) and O(5) oxygen atoms of naringenin molecule forms strong intermolecular interaction (hydrogen bonding interactions) with the binding site residues such as, Tyr435 (O(1)···H–O/Tyr435), Tyr398 (O(3)···H–O/Tyr398), Gln206 (O(3)···

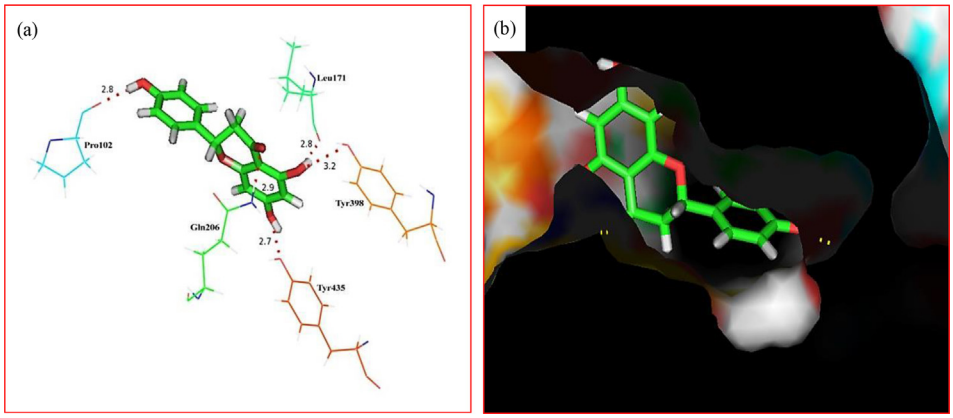

Figure 3. Showing (a) the hydrogen bonding interactions and (b) Naringenin-MAO-B complex connolly surface view plotted from QM/MM analysis.

Table 3. The topological properties of hydrogen bonding interactions of naringenin-MAO-B complex attained from the QM/MM model.

Interactions	H···A (Å)	D–H (Å)	D···A (Å)	∠D–H···A (°)	$\rho_{cp}(r)$ (eÅ^{-3})	$\nabla^2\rho_{cp}(r)$ (eÅ^{-5})	G(r) (kcal/mol)	V(r) (kcal/mol)	H(r) (kcal/mol)	D (kcal/mol)
O(5)–H(13)···O/Pro102	1.8	1.0	2.8	169.3	0.183	2.913	28.350	-37.691	-9.340	18.845
O(3)–H(3)···O(Leu171)	1.9	1.0	2.8	158.8	0.189	2.781	28.648	-39.149	-10.500	19.574
Gln206/N–H···O(4)	1.9	1.0	2.9	159.2	0.182	2.569	26.718	-36.671	-9.953	18.335
O(1)–H(1)···O/Tyr435	1.8	1.0	2.7	147.3	0.212	2.952	32.892	-46.516	-13.624	23.258

The bond angle range between 175-180° is strong, 130–180° is medium and 90–150° is weak.
The bond energy (kcal/mol) range between 14-40 is strong, 4–14 is medium and 0–4 is weak.
The distance between Donor···Acceptor is strong at 2.2–2.5, medium at 2.5–3.2 and weak at 3.2–4.0.

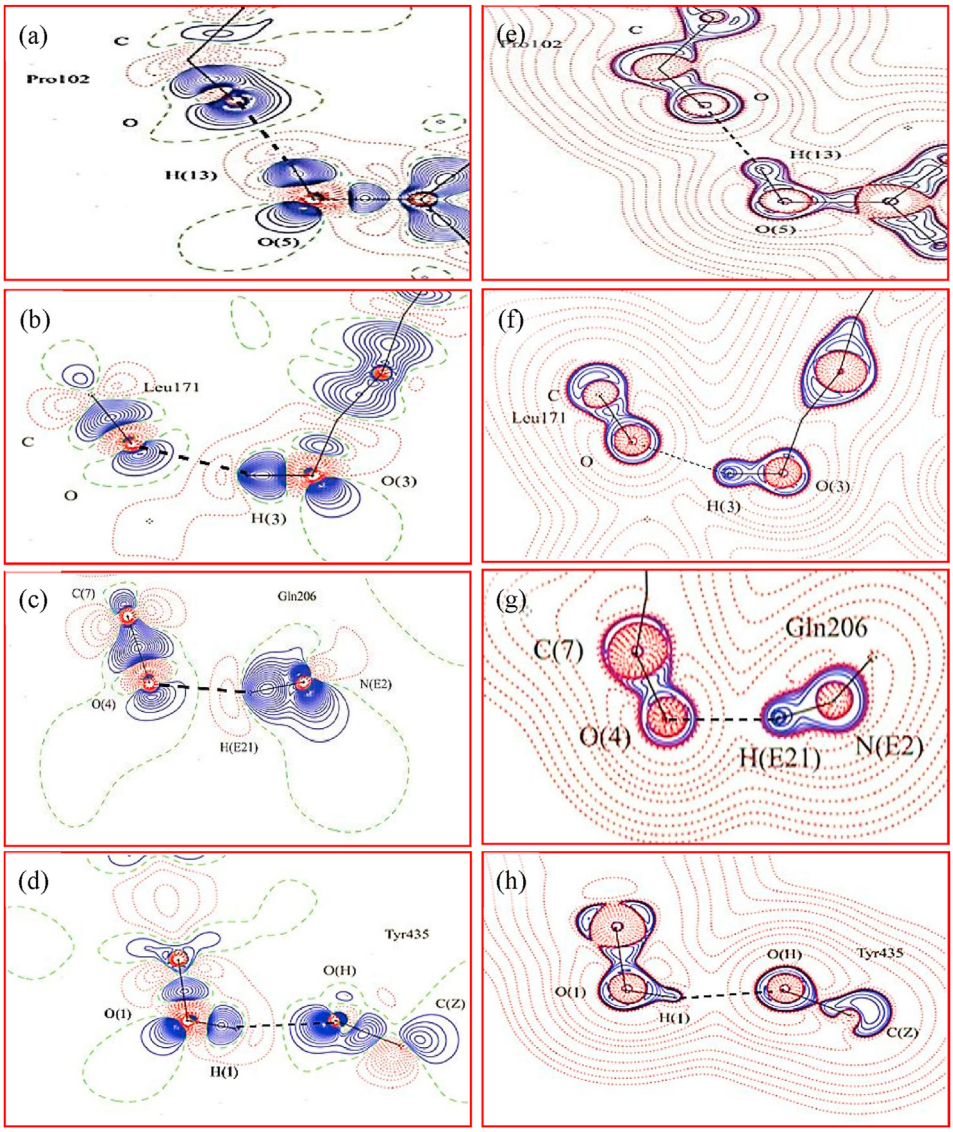

Figure 4. (a–d) displays the deformation electron density plot (Interval: 0.05 eÅ^{-3}) and (e–h) the Laplacian of electron density map drawn in 3.0 × 2^{N} eÅ^{-5} logarithmic scale, where the N = 2, 4 and 8 × 10^{n}, n = -2,-1, 0, 1, 2. The blue, red and green colours are representing the positive, negative and zero contours respectively.

H–N/Gln206), Leu171 (O(3)–H(3)···O/Leu171), Gln206 (O(4)···H–N/Gln206) and Pro102 (O(5)–H(13)···O/Pro102) at the distances of 2.9, 3.1, 3.2, 3.5, 3.0 and 3.3 Å respectively. Whereas in QM/MM, these residues are establishing the hydrogen bonding interactions with the naringenin molecule and are restrained during the QM/MM energy minimization except O(3)···H– N/Gln206 (3.9 Å) interaction. On comparing the interactions of naringenin–MAO-B complex obtained from molecular docking and QM/MM shows no significant variation (Table 2); this confirms that the conformation of naringenin molecule is not much modified and the intermolecular interactions are almost intact. Furthermore, the orient keeper residues also strongly interacts (hydrogen bonding and hydrophobic interaction) with the naringenin molecule. The hydrophobic interaction forms between O(4) atom of naringenin with the carbon atom of Tyr326 at the distance of 3.1 Å; the almost same interaction distance also observed in molecular docking (3.0 Å); this small

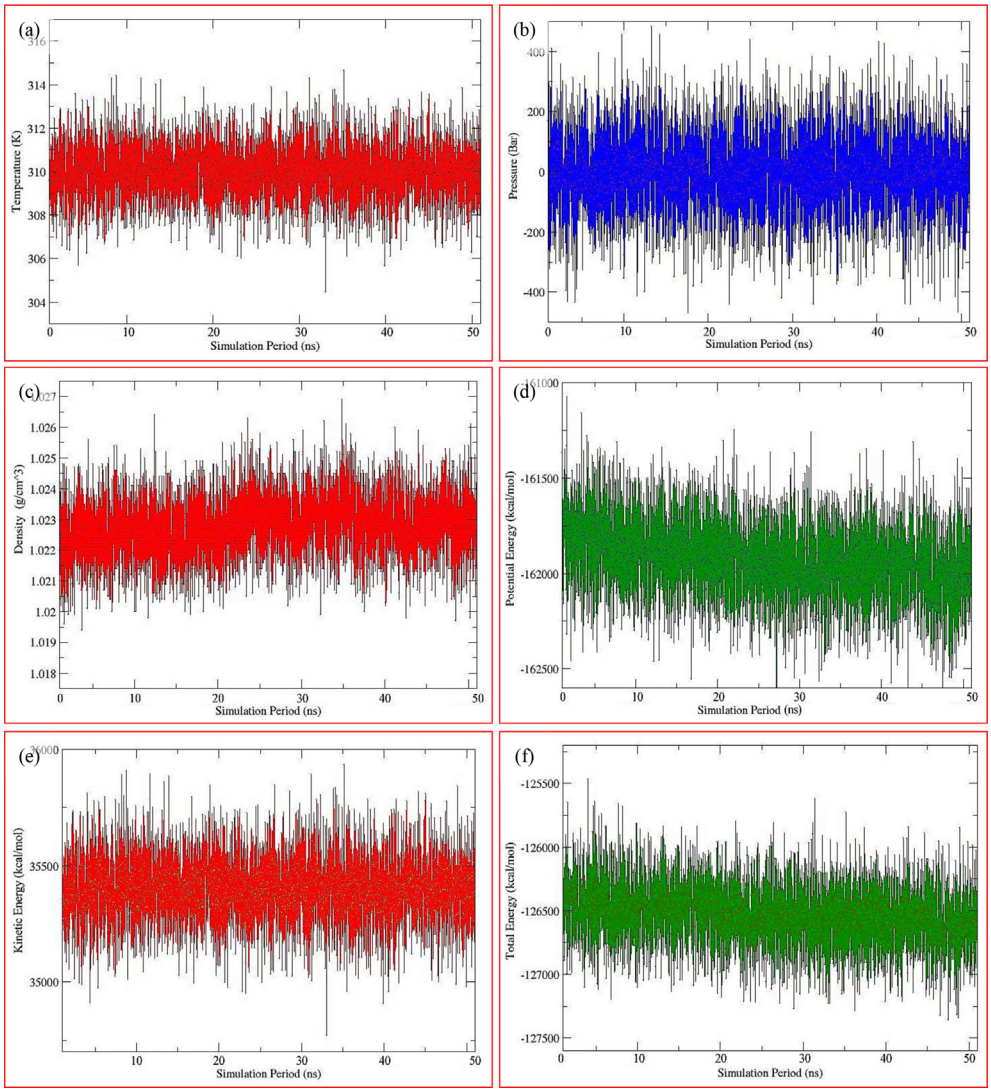

Figure 5. (a) The temperature, (b) pressure, (c) density and (d) potential energy, (e) kinetic energy and (f) total energy of naringenin-MAO-B complex during the MD simulation.

modification is attributed to the intermolecular interaction in the QM/MM region.

Furthermore, the interaction distance between the naringenin and FAD (ionization factor of MAO-B enzyme) is found to be less in QM/MM (7.8 Å) when observed with the molecular docking (8.5 Å). Figure 3(a,b) shows the intermolecular interactions of naringenin-MAO-B complex and the Connolly surface view plotted from QM/MM results. The intermolecular interactions observed from the molecular docking analysis are not significantly different from the QM/MM and the complex obtained from QM/MM method well reproduces the hydrogen bonding, hydrophobic effects and the electrostatic interactions observed in molecular docking. And this study also reveals how the naringenin molecule interacts with the orient keeper residue and the catalytic region of the MAO-B enzyme.

Using Bader theory of atoms in molecules (AIM), the intermolecular interactions of naringenin molecule in the binding pocket of MAO-B enzyme was analyzed. The QM calculation allows to predict the *cp* between interacting atoms of naringenin molecule and the binding site residues; where the non-bonded interaction charges were accumulated. The topological properties of electron density for the intermolecular interactions of naringenin-MAO-B complex have determined; the *cp*'s in intermolecular interactions region [Deformation $\rho_{cp}(r)$ and Laplacian of electron density $\nabla^2\rho_{cp}(r)$] are obtainable from Table 3. The calculated $\rho_{cp}(r)$ value of O(5)–H(13)···O/Pro102, O(3)–H(3)···O(Leu171), Gln206/N–H···O(4) and O(1)–H(1)···O/Tyr435 hydrogen bonding interactions are 0.183, 0.189, 0.182, 0.212 eÅ^{-3} [Figure 4(a-d)] and $\nabla^2\rho_{cp}(r)$ values are 2.913, 2.781, 2.569, 2.952 eÅ^{-5}respectively [Figure 4(e-h)]. The $\rho_{cp}(r)$ and $\nabla^2\rho_{cp}(r)$ values achieved from the QM/MM indicates the intermolecular interactions (hydrogen bonding interaction) are in *closed-shell* and the values are similar to the reported values [76, 77, 78]. And all the interactions are found to be strong, these values are also further confirmed from the bond dissociation energy (BDE), the corresponding values are 18.845, 19.574, 18.335 and 23.258 kcal/mol. In these, the O(1)–H(1)···O/Tyr435 intermolecular interaction displayed the positive Laplacian of electron density $\nabla^2\rho_{cp}(r)$ and relatively high deformation electron density $\rho_{cp}(r)$ and this indicate that the interaction is stronger than all other interactions. The calculated BDE value of this interaction also further confirms the strength of this bond [65, 79].

3.3. The molecular dynamics simulation of naringenin-MAO-B complex

From the IFD method, the conformer-1of naringenin-MAO-B complex was chosen to perform MD simulation. The modification in the conformation of both naringenin molecule and the residues MAO-B enzyme of the naringenin-MAO-B complex were explored from the MD simulation; this reflects the energy profile also. The thermodynamical parameters of

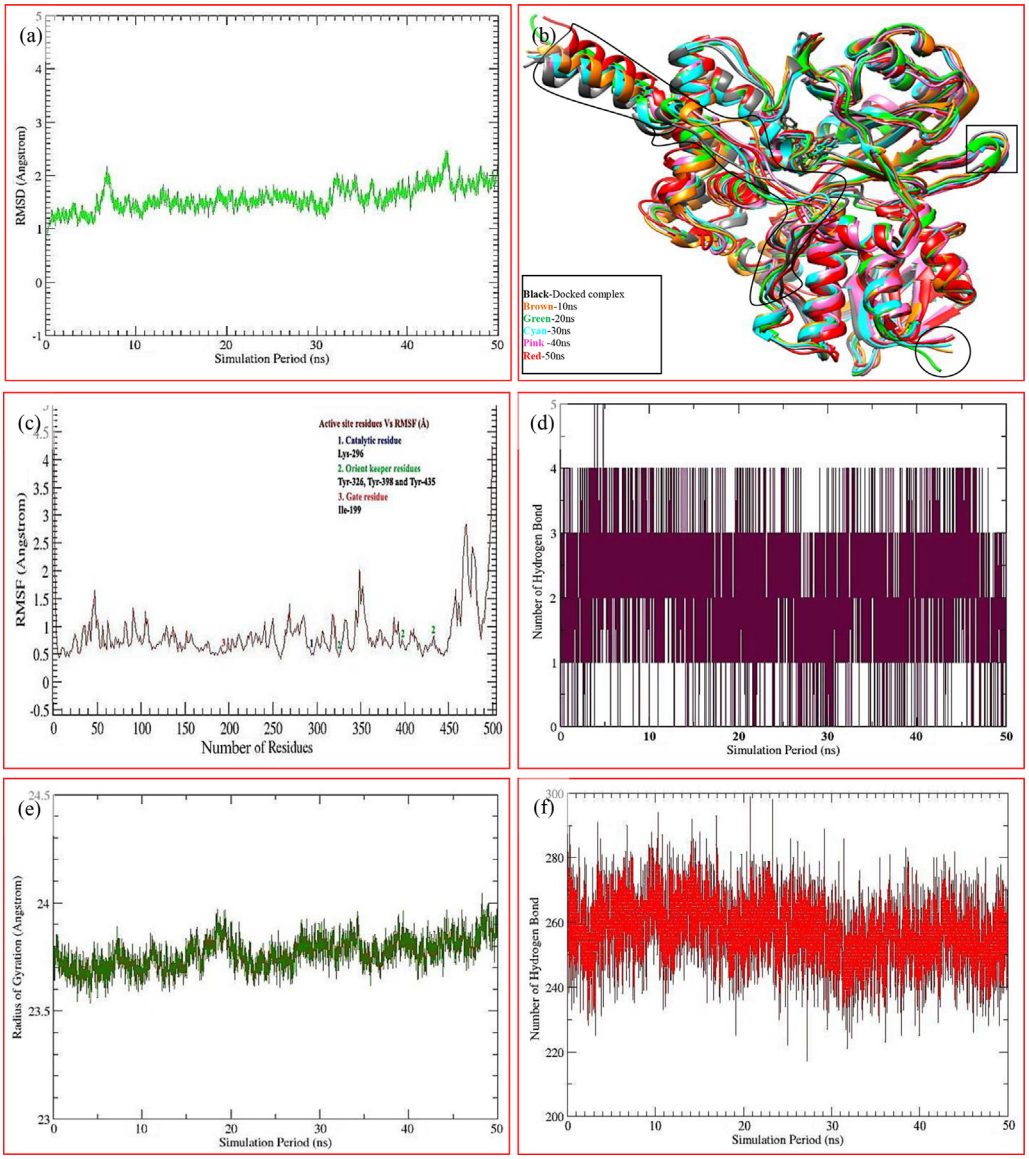

Figure 6. (a) Root mean square deviation, (b) Superimposed secondary structure poses of naringenin-MAO-B complex in docking and various stages in MD simulation, (c) Root mean square fluctuation, (d) Intermolecular hydrogen bonding interactions between naringenin molecule and MAO-B enzyme, (e) Radius of gyration and (f) intramolecular hydrogen bonding interactions of MAO-B enzyme during the MD simulation.

naringenin-MAO-B complex are shown in Figure 5(a-f). To expose the naringenin-MAO-B complex stability and conformational modification, the root mean square fluctuation (RMSF), the root mean square deviation (RMSD), radius of gyration (Rg), bond decomposition energy, binding free energy, principal component analysis (PCA), protein secondary structure elements (PSSE) and porcupine analysis are essential. These parameters were determined and analyzed.

3.3.1. *Root mean square deviation and root mean square fluctuation*

The RMSD for naringenin-MAO-B complex was carried out from MD simulation. During the MD simulation, the different stages of RMSD values have been calculated to understand the displacement of backbone atoms of naringenin-MAO-B complex with the function of time using *cpptraj module* [59]. Figure 6(a) and Figure 7(a-f) are showing the modifications in the complex conformation at molecular docking and the different stages of MD simulations. The calculated RMSD values range from 0.9 to 2.4 Å, which is almost agree with the reported results [80] and the overall variation is found to be insignificant. However, the RMSD profile indicates that the value slightly increased at 7th ns, after that the complex maintained the equilibrium state up to 50 ns (~1.0 Å) except at 43–44 ns (2.4 Å) [Figure 6(b)]; these small variations are insignificant and are not altered the conformation of naringenin-MAO-B complex. The superimposed form of naringenin-MAO-B complex reveals that the conformation of naringenin-MAO-B complex varied at various stage of MD simulation and compered with molecular docking [Figure 6(b)].

To understand the mobility of MAO-B enzyme, when naringenin molecule present in the binding site of MAO-B enzyme; the RMSF is an essential tool to explore it and the RMSF was calculated using *cpptraj module* [59]. The fluctuation of C (membrane binding region) (4.4 Å) and N-terminal (4.5 Å) regions are found to be high on compared with the other regions (0.4–2.5 Å) of MAO-B enzyme; this may be due to their anti-aquatic nature of C-terminal [Figure 6(c)]. Apart from this, the RMSF values of catalytic residues (Lys296, 0.48 Å), orient keeper residues [Tyr326 (0.48 Å), Tyr398 (0.70Å) and Tyr435 (0.82 Å)] and gate residues (Ile199, 0.56 Å) are found to be very low; this is attributed to strong contribution of intermolecular interactions with the naringenin molecule in the naringenin-MAO-B complex [Figure 6(d)].

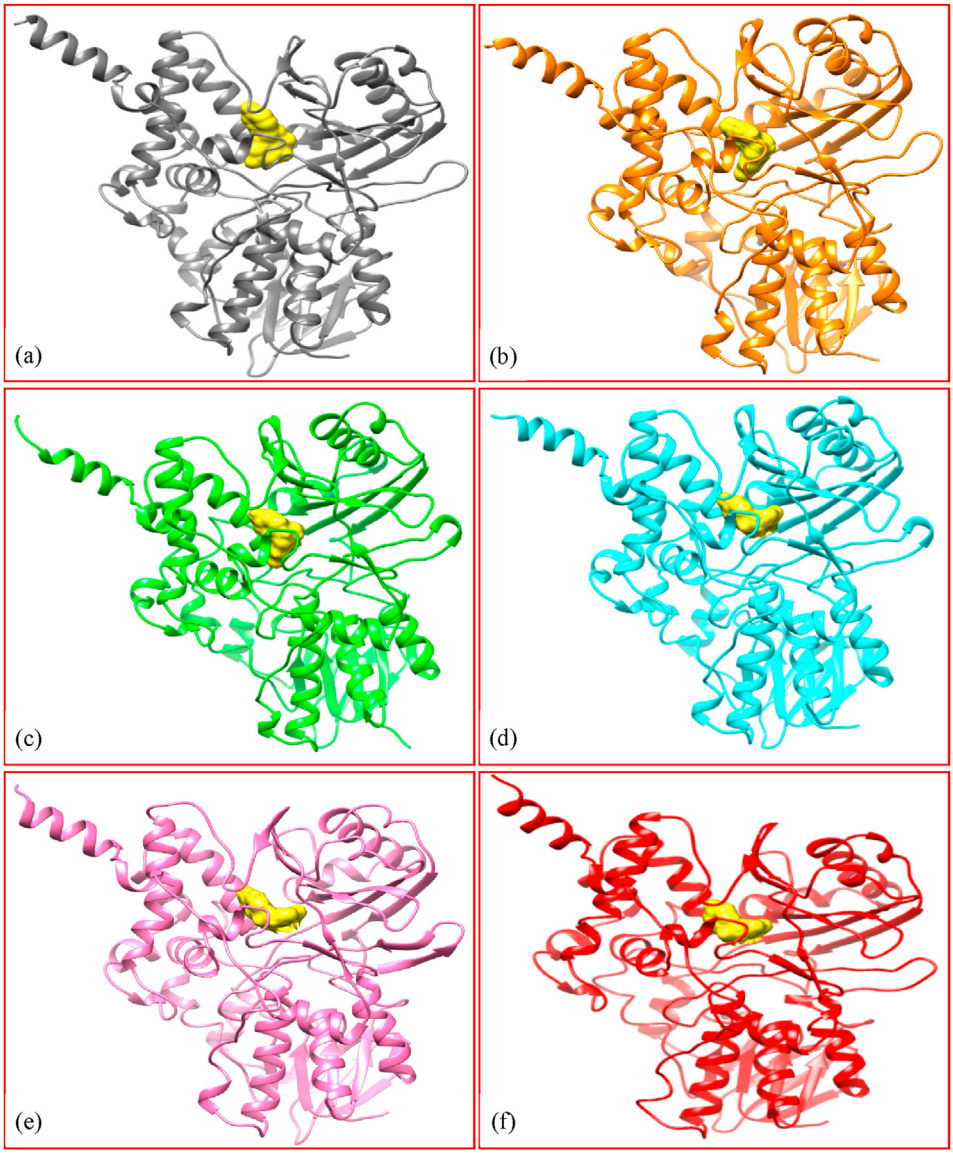

Figure 7. The conformational variations of naringenin-MAO-B complex, (a) the molecular docking (black) and (b–f) different stage (10ns-brown, 20ns-green, 30ns-cyan, 40ns-pink, and 50ns-red) of the MD simulation.

3.3.2. Rg and protein secondary structure elements

To realize the compactness of the protein, the Radius of gyration is an essential tool. The Rg values of MAO-B enzyme was calculated with the function of simulation time [Figure 6(e)]. The *cpptraj module* was used to calculate the Rg values of naringenin-MAO-B complex [59]. The Rg value of naringenin-MAO-B complex shows high compactness (~23.75Å) on compared with the reported value (~25 Å) [81]. From the Figure 6(e-f), it is observed that during the molecular dynamics simulation, the Rg value of naringenin-MAO-B complex varies between 23.6 to 24.1 Å and the maximum deviation is found ~0.5 Å; this reveals that the MAO-B enzyme is highly compact. This is due to the intra-molecular hydrogen bonding interactions (number of H-bond interactions is ~260) of MAO-B enzyme shown in Figure 6(f).

The protein secondary structure elements (PSSE) analysis (beta-strands, beta-sheets, beta turn, 3–10 helix and alpha-helix) are essential to confirm the conformational modification of protein. Figure 8(a) displays the PSSE of naringenin-MAO-B complex obtained from the MD simulations, reveal the secondary structure variation of naringenin-MAO-B complex. In which, the conformation of C, N-terminals, loop, S-bend, and T-turn residues are significantly modified during the simulation [Figure 8(b)]. However, this modification not affects the compactness of enzyme.

3.3.3. Intermolecular interactions

The atomic level binding information is essential to explore the binding properties of the naringenin in the binding site of MAO-B enzyme. The intermolecular interactions of naringenin with substrate binding site (orient keep residues and catalytic residue) and gate residues of MAO-B enzyme allows to explicit the mechanism of MAO-B enzyme inhibition. In molecular docking, the O(4) atom of naringenin molecule interacts with the orient keeper residues Tyr326 at the distance of 3.0 Å; this interaction was retained during the QM/MM and MD simulations, the corresponding distances are 3.1 and 3.0 Å. The catalytic amino acid Lys296 forms interaction with the FAD binding domain and this is responsible to oxidize the FAD coenzyme. In molecular docking, the Lys296 forms interactions with FAD at the distance of 3.5 Å; whereas in MD simulation, this interaction was altered and the distance has been increased to 6.4 Å and it doesn't sufficient to initiate the ionization process of FAD coenzyme.

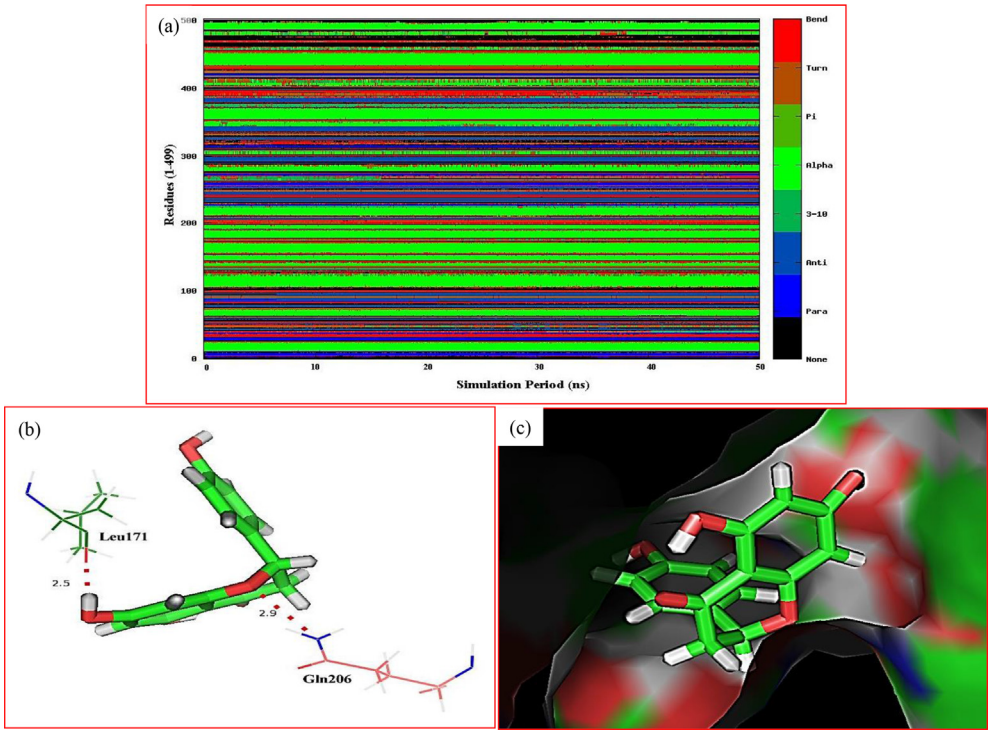

Figure 8. (a) The protein secondary structure element obtained from the MD simulation, (b) the intermolecular hydrogen bonding interactions of naringenin-MAO-B complex and (c) Connolly surface map of complex plotted from the MD simulations.

The conformation of naringenin is significantly modified, when the complex appears in the MD simulation; it alters the intermolecular interaction of naringenin molecules with the binding site residues of MAO-B enzyme. In QM/MM and molecular docking, the O(3) atom of naringenin molecule appears a hydrogen bonding interaction with Leu171 [O(3)–H(3)···Leu171/O] at the distances of 3.5 and 2.8 Å respectively. This interaction was disappeared in MD simulation, the corresponding distance is 6.3 Å. And the O(1) atom of naringenin also interacts with Leu171 and formed hydrogen bonding interactions [O(1)–H(1)···Leu171/O], the interaction distance found in MD simulation is 2.5 Å. Similarly, in molecular docking, the O(3), O(4) atoms of naringenin molecule formed intermolecular interaction with Glu206 at the distance of 3.0 and 3.2 Å respectively (hydrogen bonding interaction); whereas, in MD simulation these interactions were disappeared (6.4, 5.3 Å). Alternately, the O(2) oxygen atom of naringenin molecule formed

Table 4. Calculated binding free energy values (kcal/mol) of naringenin-MAO-B complexes using MM-GBSA methods.

Contribution	MM-GBSA
E_{vdw}	-38.45±2.15
E_{ele}	-20.00±2.31
ΔG_{GB}	32.45±2.85
ΔG_{SA}	-4.87±0.14
ΔG_{gas}	-58.46±2.45
ΔG_{solv}	27.57±1.66
ΔG_{Total}	-30.87±1.98
$T\Delta S$	-18.04±6.25
ΔG	-12.83±4.11

ΔG– Total binding free energy.
ΔG_{Total} –Total Binding free energy without entropic contribution.
TΔS– Conformational entropy change upon ligand binding.
ΔG_{solv} – Total polar solvation contribution in the binding free energy
ΔG_{GB}– Polar solvation contribution in the binding free energy.
ΔG_{gas} –Total polar solvation contribution in the binding free energy.
E_{SA}–Non polar solvation contribution in the binding free energy.
E_{vdw} – van der Waals contribution in the binding free energy.
E_{ele}–Electrostatic contribution in the binding free energy.

Table 5. The decomposition energy (kcal/mol) of individual contributions of binding site residues for the ligand binding from the MM-GBSA calculation.

Residues	ΔE_{vdw}	ΔE_{ele}	ΔG_{GB}	ΔG_{SA}	ΔG_{Total}
Phe99	-0.02	0.06	-0.04	0.0	0.0
Pro102	-0.05	-0.32	0.38	0.0	0.0
Phe103	-0.04	0.10	-0.11	0.0	-0.04
Pro104	-0.06	0.08	-0.05	-0.01	-0.04
Trp119	-0.10	0.0	0.09	-0.01	-0.02
Leu164	-0.05	0.08	-0.09	0.0	-0.06
Leu167	-0.25	0.06	-0.33	0.0	-0.52
Phe168	-1.12	-0.86	0.59	-0.06	-1.46
Leu171	-1.97	-4.96	2.81	-0.28	-4.41
Cys172	-1.15	0.0	0.28	-0.05	-0.92
Tyr188	-0.05	0.04	0.00	0.0	0.0
Ile198	-1.21	-0.89	1.21	-0.10	-0.99
Ile199	-1.95	-0.45	0.68	-0.20	-1.91
Ser200	-0.17	-0.18	0.28	-0.01	-0.08
Thr201	-0.12	-0.01	0.07	0.0	-0.06
Gln206	-1.72	0.44	0.45	-0.23	-1.06
Ile316	-0.41	-0.01	-0.04	-0.08	-0.56
Tyr326	-2.34	-0.58	1.38	-0.24	-1.78
Leu328	-0.45	0.02	0.0	-0.06	-0.48
Phe343	-0.93	-0.04	0.41	-0.12	-0.67
Tyr398	-0.67	0.65	-0.28	-0.02	-0.33
Trp432	-0.02	0.04	-0.06	0.0	-0.04
Tyr435	-0.28	0.05	0.14	0.0	-0.09
Fad	-1.19	0.0	0	-0.11	-1.30

intermolecular interaction with Glu206 (2.9 Å) during the MD simulation [Table 2 and Figure 8(b)]. These interactions keep the naringenin molecule in the substrate binding cavity [Figure 8(c)] [8, 20, 82, 83].

3.3.4. Binding free energy and decomposition energy analysis

To understand the conformational stability of the complex based on its binding energy, the binding free energy was calculated; which is a well-known method to predict the energy contributed to form the ligand-protein complex. The summation of solvation free energy and gas phase energy were taken place to find out the total binding energy of naringenin-MAO-B complex. The sum of electrostatic (-20.00± 2.31 kcal/mol) and van der Waals (-38.45±2.15 kcal/mol) energies is equal to gas-phase (ΔG_{gas} = -58.46 ± 2.45 kcal/mol) interaction energy. Similarly, the solvation free energy ($\Delta G_{solvation}$ = 27.57± 1.66 kcal/mol) is the sum of polar (ΔG_{GB} = 32.45±2.85 kcal/mol) and non-polar (ΔG_{SA} = -4.87±0.14 kcal/mol) contribution. In the total binding free energy values (−30.87 ± 1.9 kcal/mol), the van der Waals energy is the dominant factor; which is calculated using the MM/GBSA methods [Table 4]. From the difference of enthalpy(ΔH) and entropy(ΔS) contribution, the total binding free energy(ΔG) is calculated.

$$\Delta G = \Delta H - T\Delta S$$

The entropy (TΔS) was determined from the n-mode analysis, the calculated value of the same is -18.04 ± 6.25 kcal/mol and the calculated binding free energy is ΔG = -12.83 ± 4.11 kcal/mol. These values indicate that the naringenin-MAO-B complex displays high binding conformational stability and these values are relatively high on compared with the reported values [84, 85].

The individual contribution of the each residue in ligand binding was calculated using the decomposition energy analysis. Using MM-GBSA method, the decomposition energy was calculated from the non-bonded interaction of naringenin with the binding site residues of MAO-B enzyme (Table5). On comparing all other interaction energies, the van der Waals interaction energies is highly contributed. The highest involvement of Leu171 (-4.96 kcal/mol) is spread the interaction in the ligand binding compared with the other binding site residues; this influence may be due to the strong hydrogen bonding interactions during the MD simulation. Moreover, the other binding site residues are also subsidized to make the naringenin-MAO-B complex strong; such residues are gate residue of Ile199 (-1.91 kcal/mol), orient keeper residues Tyr326 (-1.78 kcal/mol), Gln206 (-1.06 kcal/mol) and the cofactor FAD (-1.30 kcal/mol), in which the FAD is responsible for

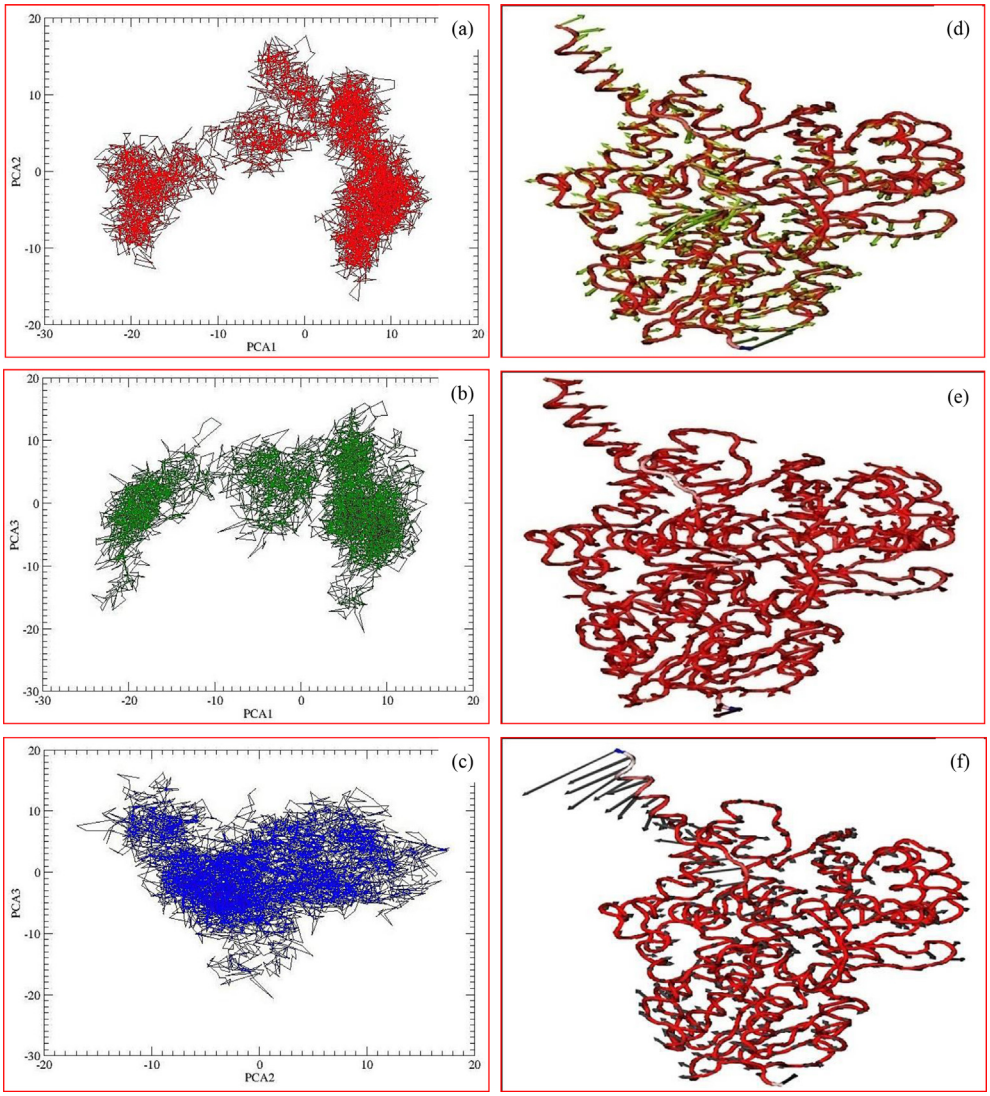

Figure 9. Projection of the motion of the Naringenin-MAO-B complex in the phase space along the (a) first two, (b) first and third, (c) second and third principal eigen vectors at 300 K and (d–f) the corresponding projection vectors are represented in *porcupine* plot.

the ionization of the substrate molecule. The results of both binding free energy and decomposition energy analysis are found similar to the recent reports [21, 85].

3.3.5. Principal component analysis

The flexibility of protein structure was analyzed using PCA; which is the most frequently used method often used for the bio-molecules like Protein, DNA and RNA. To correlate the molecular motion of N-atom, the PCA is necessary in the MD simulation. The covariance matrix calculation and thus obtained eigenvectors and eigenvalues provide the fluctuation of backbone Cα atom during the MD simulation. In the present study, the first three principal components of naringenin-MAO-B complex are highly contributed for positional motion of the Cα atom. The PC1, PC2 and PC3 values of naringenin-MAO-B complex are 39.9, 14.5 and 10.5% respectively. The first three modes are contributing ~65% protein motion, this is shown in Figure 9(a-c), in which, the complex shows high dynamic in nature for PCA1-PCA2 and PCA1-PCA3; whereas in PCA2-PCA3, the complex is slightly rigid. This analysis reveals that the naringenin-MAO-B complex is considerably flexible. Furthermore, the *porcupine* plot was created for naringenin-MAO-B complex through the analysis of eigenvectors. The third mode has high flexibility and mobility compared with all other modes; this is clearly shown in Figure 9(d-f).

4. Conclusion

The computational analysis reveals that the flavonoid family of naringenin displays the orientation and conformational consistency of the molecule in the binding site of MAO-B enzyme. The molecular docking results obtained from the IFD method shows the naringenin has high binding affinity with binding site residues of MAO-B enzyme. The glide energy (-51.074 kcal/mol), docking score (-12.029 kcal/mol), prime energy (-21690.8 kcal/mol) and IFD score (-1096.57 kcal/mol) of naringenin confirms that it has high binding affinity towards MAO-B enzyme. In molecular docking, the oxygen atoms [O(1), O(2), O(3), O(4) and O(5)] of naringenin molecule forms hydrophobic and hydrogen bonding interactions with the catalytic residue, FAD, gate residue and orient keeper residues; this indicates that naringenin has strong binding affinity towards the MAO-B enzyme. During the MD simulation, these interactions are very stable and also keep the naringenin molecule in the binding site, which leads to stop the ionization process of MAO-B enzyme. Furthermore, the MD simulation of naringenin-MAO-B complex reveals that the thermodynamic properties and energy profiles were stable. Moreover, the low values of RMSD and RMSF confirms the stability of naringenin in the binding site of MAO-B enzyme. In MD simulation, the O(1) and O(2) atoms of naringenin forms hydrogen bonding interaction with Leu171 and Glu206 and are stable throughout the simulation. Here, the O(1) atom blocks the Leu171 and Tyr398 residues; this facilitates to block the function of MAO-B enzyme. These structural details suggest that the naringenin molecule potentially inhibits the MAO-B enzyme.

Declarations

Author contribution statement

Govindasamy Hunday: Conceived and designed the experiments; Performed the experiments; Analyzed and interpreted the data; Contributed reagents, materials, analysis tools or data; Wrote the paper.

Magudeeswaran Sivanandam: Performed the experiments.

Kandasamy Saravanan: Analyzed and interpreted the data.

Poomani Kumaradhas: Conceived and designed the experiments; Contributed reagents, materials, analysis tools or data; Wrote the paper.

Funding statement

This research did not receive any specific grant from funding agencies in the public, commercial, or not-for-profit sectors.

Data availability statement

The data that has been used is confidential.

Declaration of interests statement

The authors declare no conflict of interest.

Additional information

No additional information is available for this paper.

Acknowledgements

The authors thank to Computer Centre, Periyar University for providing HPC facility Sponsored by RUSA (Rashtriya Uchchatar Shiksha Abhiyan) to perform the docking and MD simulation.

References

[1] S.P. William Dauer, Mechanisms and models, cambridge companion to, Philos. Biol. 39 (2007) 139–159.
[2] F.N. Emamzadeh, A. Surguchov, Parkinson's disease: biomarkers, treatment, and risk factors, Front. Neurosci. 12 (2018) 1–14.
[3] J.M. Shulman, P.L. De Jager, M.B. Feany, Parkinson's disease: genetics and pathogenesis, Annu. Rev. Pathol. Mech. Dis. 6 (2011) 193–222.
[4] S. Andalib, M.S. Vafaee, A. Gjedde, Parkinson's disease and mitochondrial gene variations: a review, J. Neurol. Sci. 346 (2014) 11–19.
[5] R. Skelly, L. Brown, A. Fakis, R. Walker, Hospitalization in Parkinson's disease: a survey of UK neurologists, geriatricians and Parkinson's disease nurse specialists, Park. Relat. Disord. 21 (2015) 277–281.
[6] A.V. Veselovsky, A.S. Ivanov, A.E. Medvedev, Computer modelling and visualization of active site of monoamine oxidases, Neurotoxicology 25 (2004) 37–46.
[7] K.L. Kirk, S. Yoshida, G.D. Haufe, Synthesis and Biochemical Evaluation of Fluorinated Monoamine Oxidase Inhibitors, 2008.
[8] A. Holt, M.D. Berry, A.A. Boulton, On the binding of monoamine oxidase inhibitors to some sites distinct from the MAO active site, and effects thereby elicited, Neurotoxicology 25 (2004) 251–266.
[9] A. Prah, E. Frančišković, J. Mavri, J. Stare, Electrostatics as the driving force behind the catalytic function of the monoamine oxidase A enzyme confirmed by quantum computations, ACS Catal. 9 (2019) 1231–1240.
[10] H. Gaweska, P.F. Fitzpatrick, Structures and mechanism of the monoamine oxidase family, Biomol. Concepts 2 (2011) 365–377.
[11] M. Li, C. Binda, A. Mattevi, D.E. Edmondson, Functional role of the "aromatic cage" in human monoamine oxidase B: structures and catalytic properties of Tyr435 mutant proteins, Biochemistry 45 (2006) 4775–4784.
[12] S.-Y. Son, J. Ma, Y. Kondou, M. Yoshimura, E. Yamashita, T. Tsukihara, Structure of human monoamine oxidase A at 2.2-Å resolution: the control of opening the entry for substrates/inhibitors Se-Young 105 (2008) 5739–5744.
[13] R. Vianello, M. Repic, How are biogenic amines metabolized by monoamine oxidases? Eur. J. Org Chem. (2012) 7057–7065.
[14] E. Abad, R.K. Zenn, J. Ka, Reaction mechanism of monoamine oxidase from QM/MM Calculations, J. Phys. Chem. B (2013) 14238–14246.
[15] V.E. Atalay, S.S. Erdem, A comparative computational investigation on the proton and hydride transfer mechanisms of monoamine oxidase using model molecules, Comput. Biol. Chem. 47 (2013) 181–191.
[16] G. Zapata-torres, A. Fierro-huerta, G. Barriga, J.C. Salgado, C.A. Celis-barros, G. Zapata-torres, Revealing monoamine oxidase B catalytic mechanisms by means of quantum chemical cluster Approach corresponding Author : J. Chem. Inf. Model. 1349 (2015).
[17] G. Oanca, J.S., Miha Purg, Janez Mavri, Jean C. Shihd, Insights into enzyme point mutation effect by molecular simulation: phenylethylamine, Phys. Chem. Chem. Phys. (2016).
[18] M. Poberžnik, M. Purg, M. Repič, J. Mavri, R. Vianello, Empirical valence bond simulations of the hydride-transfer step in the monoamine oxidase a catalyzed metabolism of noradrenaline, J. Phys. Chem. B 120 (2016) 11419–11427.
[19] D. Pregeljc, J. Mavri, J. Stare, Why does the Y326I mutant of monoamine oxidase B decompose an endogenous amphetamine at a slower rate than the wild type

enzyme ? Reaction step elucidated by multiscale molecular simulations, Phys. Chem. Chem. Phys. (2018) 4181.
[20] T. Tandaric, R. Vianello, Computational Insight into the Mechanism of the Irreversible Inhibition of Monoamine Oxidase Enzymes by the Antiparkinsonian Propargylamine Inhibitors Rasagiline and Selegiline, 2019.
[21] T. Tandarić, A. Prah, J. Stare, J. Mavri, R. Vianello, Hydride abstraction as the rate-limiting step of the irreversible inhibition of monoamine oxidase b by rasagiline and selegiline: a computational empirical valence bond study, Int. J. Mol. Sci. 21 (2020) 1–13.
[22] M.B.H. Youdim, D. Edmondson, K.F. Tipton, The therapeutic potential of monoamine oxidase inhibitors, Nat. Rev. Neurosci. 7 (2006) 295–309.
[23] C. Binda, F. Hubálek, M. Li, Y. Herzig, J. Sterling, D.E. Edmondson, A. Mattevi, Crystal structures of monoamine oxidase B in complex with four inhibitors of the N-propargylaminoindan class, J. Med. Chem. 47 (2004) 1767–1774.
[24] G.I. Stafford, M.E. Pedersen, J. van Staden, A.K. Jäger, Review on plants with CNS-effects used in traditional South African medicine against mental diseases, J. Ethnopharmacol. 119 (2008) 513–537.
[25] I. Erlund, Review of the flavonoids quercetin, hesperetin, and naringenin. Dietary sources, bioactivities, bioavailability, and epidemiology, Nutr. Res. 24 (2004) 851–874.
[26] R.N. Jadeja, R.V. Devkar, Polyphenols and Flavonoids in Controlling Non-alcoholic Steatohepatitis, Elsevier Inc., 2013.
[27] L. Hritcu, R. Ionita, P.A. Postu, G.K. Gupta, H. Turkez, T.C. Lima, C.U.S. Carvalho, D.P. de Sousa, Antidepressant flavonoids and their relationship with oxidative stress, Oxid. Med. Cell. Longev. (2017) (2017) 1–18.
[28] A.L. Simons, R. Mathieu, P.A. Murphy, H. Suzanne, Greater apparent absorption of flavonoids is associated with lesser human fecal flavonoid disappearance rates, J. Agric. Food Chem. 58 (2010) 141–147.
[29] M.A. Alam, N. Subhan, M.M. Rahman, S.J. Uddin, H.M. Reza, S.D. Sarker, Effect of citrus flavonoids, naringin and naringenin, on metabolic syndrome and their mechanisms of action, Adv. Nutr. 5 (2014) 404–417.
[30] E.E. Mulvihill, E.M. Allister, B.G. Sutherland, D.E. Telford, C.G. Sawyez, J.Y. Edwards, J.M. Markle, R. a Hegele, Receptor – null mice with diet-induced insulin resistance, Diabetes 58 (2009) 2198–2210.
[31] H.L. Chang, Y.M. Chang, S.C. Lai, K.M. Chen, K.C. Wang, T.T. Chiu, F.H. Chang, L.S. Hsu, Naringenin inhibits migration of lung cancer cells via the inhibition of matrix metalloproteinases-2 and-9, Exp. Ther. Med. 13 (2017) 739–744.
[32] Y. Nahmias, J. Goldwasser, M. Casali, D. Van Poll, T. Wakita, R.T. Chung, M.L. Yarmush, Apolipoprotein B-dependent hepatitis C virus secretion is inhibited by the grapefruit flavonoid naringenin, Hepatology 47 (2008) 1437–1445.
[33] A.S.C. Wenjie Jessie Lu, Valentina ferlito, Cong Xu, David Alastair, Flockhart, enantiomers of naringenin as pleiotropic, stereoselective inhibitors of cytochrome P450 isoforms WENJIE, Chirality 26 (2014) 553–562.
[34] B. Salehi, P.V.T. Fokou, M. Sharifi-Rad, P. Zucca, R. Pezzani, N. Martins, J. Sharifi-Rad, The therapeutic potential of naringenin: a review of clinical trials, Pharmaceuticals 12 (2019) 1–18.
[35] V.V. Vj, S. Ar, S.K. Mn, Role of Naringin and Naringenin in various diseased conditions, Int. J. Pharm. Res. Sch. 2 (2013) 198–212.
[36] K. Wang, Z. Chen, L. Huang, B. Meng, X. Zhou, X. Wen, D. Ren, Naringenin reduces oxidative stress and improves mitochondrial dysfunction via activation of the Nrf2/ARE signaling pathway in neurons, Int. J. Mol. Med. 40 (2017) 1582–1590.
[37] S.L. Kinnings, N. Liu, N. Buchmeier, P.J. Tonge, L. Xie, P.E. Bourne, Drug discovery using chemical systems biology: repositioning the safe medicine Comtan to treat multi-drug and extensively drug resistant tuberculosis, PLoS Comput. Biol. 5 (2009).
[38] E.I. Mohamed, M.A. Zaki, N.D. Chaurasiya, A.I. Owis, S. AbouZid, Y.H. Wang, B. Avula, A.A. Seida, B.L. Tekwani, S.A. Ross, Monoamine oxidases inhibitors from Colvillea racemosa: isolation, biological evaluation, and computational study, Fitoterapia 124 (2018) 217–223.
[39] M.J. Frisch, G.W. Trucks, H.B. Schlegel, G.E. Scuseria, M.A. Robb, J.R. Cheeseman, G. Scalmani, V. Barone, B. Mennucci, G.A. Petersson, H. Nakatsuji, M. Caricato, X. Li, H.P. Hratchian, A.F. Izmaylov, J. Bloino, G. Zheng, J.L. Sonnenberg, M. Hada, M. Ehara, K. Toyota, R. Fukuda, J. Hasegawa, M. Ishida, T. Nakajima, Y. Honda, O. Kitao, H. Nakai, T. Vreven, J.A. Montgomery, J.E. Peralta, F. Ogliaro, M. Bearpark, J.J. Heyd, E. Brothers, K.N. Kudin, V.N. Staroverov, T. Keith, R. Kobayashi, J. Normand, K. Raghavachari, A. Rendell, J.C. Burant, S.S. Iyengar, J. Tomasi, M. Cossi, N. Rega, J.M. Millam, M. Klene, J.E. Knox, J.B. Cross, V. Bakken, C. Adamo, J. Jaramillo, R. Gomperts, R.E. Stratmann, O. Yazyev, A.J. Austin, R. Cammi, C. Pomelli, J.W. Ochterski, R.L. Martin, K. Morokuma, V.G. Zakrzewski, G.A. Voth, P. Salvador, J.J. Dannenberg, S. Dapprich, A.D. Daniels, O. Farkas, J.B. Foresman, J.V. Ortiz, J. Cioslowski, D.J. Fox, J.A. Montgomery Jr., J.E. Peralta, F. Ogliaro, M. Bearpark, J.J. Heyd, E. Brothers, K.N. Kudin, V.N. Staroverov, R. Kobayashi, J. Normand, K. Raghavachari, A. Rendell, J.C. Burant, S.S. Iyengar, J. Tomasi, M. Cossi, N. Rega, J.M. Millam, M. Klene, J.E. Knox, J.B. Cross, V. Bakken, C. Adamo, J. Jaramillo, R. Gomperts, R.E. Stratmann, O. Yazyev, A.J. Austin, R. Cammi, C. Pomelli, J.W. Ochterski, R.L. Martin, K. Morokuma, V.G. Zakrzewski, G.A. Voth, P. Salvador, J.J. Dannenberg, S. Dapprich, A.D. Daniels, Ö. Farkas, J.B. Foresman, J.V. Ortiz, J. Cioslowski, D.J. Fox, Gaussian 09, Revision D.01, Gaussian Inc, 2013, pp. 1–20.
[40] R.J. Boyd, The development of computational chemistry in Canada, Rev. Comp. Chem. (2007) 213–299.
[41] G.M. Sastry, M. Adzhigirey, W. Sherman, Protein and Ligand Preparation : Parameters , Protocols , and Influence on Virtual Screening Enrichments, 2013, pp. 221–234.
[42] W.L. Jorgensen, D.S. Maxwell, J. Tirado-rives, Development and testing of the OPLS all-atom force field on conformational energetics and properties of organic liquids 7863 (1996) 11225–11236.
[43] T.A. Halgren, Identifying and characterizing binding sites and assessing druggability, J. Chem. Inf. Model. 49 (2009) 377–389.
[44] R. Farid, T. Day, A. Friesner, R.A. Pearlstein, New insights about HERG blockade obtained from protein modeling , potential energy mapping , and docking studies 14 (2006) 3160–3173.
[45] W. Sherman, T. Day, M.P. Jacobson, R.A. Friesner, R. Farid, Novel procedure for modeling ligand/receptor induced fit effects, J. Med. Chem. 49 (2006) 534–553.
[46] W. DeLano, PyMOL : an Open-Oource Molecular Graphics Tool, CCP4 Newsl. Protein Crystallogr, 2002.
[47] E.F. Pettersen, T.D. Goddard, C.C. Huang, G.S. Couch, D.M. Greenblatt, E.C. Meng, T.E. Ferrin, UCSF Chimera - a visualization system for exploratory research and analysis, J. Comput. Chem. 25 (2004) 1605–1612.
[48] A.C. Wallace, R.A. Laskowski, J.M. Thornton, LIGPLOT : a program to generate schematic diagrams of protein-ligand interactions Clean up structure 8 (1995) 127–134.
[49] J. Wang, R.M. Wolf, J.W. Caldwell, P.A. Kollman, D.A. Case, Development and testing of a general Amber force field, J. Comput. Chem. 25 (2004) 1157–1174.
[50] J.A. Maier, C. Simmerling, L. Wickstrom, K.E. Hauser, C. Martinez, K. Kasavajhala, ff14SB: improving the accuracy of protein side chain and backbone parameters from ff99SB, J. Chem. Theor. Comput. 11 (2015) 3696–3713.
[51] J. Wang, W. Wang, P.A. Kollman, D.A. Case, Antechamber , an accessory software package for molecular mechanical calculations, Molecules 222 (2001). U403–U403.
[52] P. Mark, L. Nilsson, Structure and dynamics of the TIP3P, SPC, and SPC/E water models at 298 K, J. Phys. Chem. A. 105 (2001) 9954–9960.
[53] M.F. Harrach, B. Drossel, Structure and dynamics of TIP3P, TIP4P, and TIP5P water near smooth and atomistic walls of different hydroaffinity, J. Chem. Phys. 140 (2014).
[54] D.A. Case, T. Darden, T.E.C. Iii, C. Simmerling, S. Brook, A. Roitberg, J. Wang, U.T. Southwestern, R.E. Duke, U. Hill, R. Luo, U.C. Irvine, D.R. Roe, R.C. Walker, S. Legrand, J. Swails, D. Cerutti, J. Kaus, R. Betz, R.M. Wolf, K.M. Merz, M. State, G. Seabra, P. Janowski, F. Paesani, J. Liu, X. Wu, T. Steinbrecher, H. Gohlke, N. Homeyer, Q. Cai, U.C. Irvine, W. Smith, U.C. Irvine, D. Mathews, R. Salomon-ferrer, C. Sagui, N.C. State, V. Babin, N.C. State, T. Luchko, S. Gusarov, A. Kovalenko, J. Berryman, P.A. Kollman, U.C.S. Francisco, Amber 14 Manual, Univ. California, San Fr, 2014. http://www.ambermd.org.
[55] G.J. Martyna, A. Hughes, M.E. Tuckerman, Molecular dynamics algorithms for path integrals at constant pressure, J. Chem. Phys. 110 (1999) 3275–3290.
[56] A. Jones, B. Leimkuhler, Adaptive stochastic methods for sampling driven molecular systems, J. Chem. Phys. 135 (2011).
[57] H.J.C. Berendsen, J.P.M. Postma, W.F. Van Gunsteren, A. Dinola, J.R. Haak, Molecular dynamics with coupling to an external bath, J. Chem. Phys. 81 (1984) 3684–3690.
[58] J.P. Ryckaert, G. Ciccotti, H.J.C. Berendsen, Numerical integration of the cartesian equations of motion of a system with constraints: molecular dynamics of n-alkanes, J. Comput. Phys. 23 (1977) 327–341.
[59] D.R. Roe, T.E. Cheatham, PTRAJ and CPPTRAJ: software for processing and analysis of molecular dynamics trajectory data, J. Chem. Theor. Comput. 9 (2013) 3084–3095.
[60] Paul J Turner and ACE/gr development team, P.J.T. and A. development team, Xmgr: List of changes, 1998, pp. 1–11. http://plasma-gate.weizmann.ac.il/Xmgr/doc/CHANGES.html.
[61] W. Humphrey, A. Dalke, K. Schulten, VMD: visual molecular dynamics, J. Mol. Graph. 14 (1996) 33–38.
[62] M. Sivanandam, S. Manjula, P. Kumaradhas, Investigation of activation mechanism and conformational stability of N-(4-chloro-3-trifluoromethyl-phenyl)-2-ethoxybenzamide and N-(4-chloro-3-trifluoromethyl-phenyl)-2-ethoxy-6-pentadecyl-benzamide in the: active site of p300 histone acetyl transferase, J. Biomol. Struct. Dyn. (2019) 1–13.
[63] P. Sivakumar, R. Niranjana Devi, S. Israel, G. Chakkaravarthi, 3-Methylpyridinium 4-nitrobenzoate–4-nitrobenzoic acid (1/1), IUCrData 1 (2016).
[64] J. Naudts, E. Van Der Straeten, A generalized quantum microcanonical ensemble, J. Stat. Mech. Theory Exp. 6015 (2006).
[65] K. Saravanan, M. Sivanandam, G. Hunday, L. Mathiyalagan, P. Kumaradhas, Investigation of intermolecular interactions and stability of verubecestat in the active site of BACE1: development of first model from QM/MM-based charge density and MD analysis, J. Biomol. Struct. Dyn. (2018).
[66] R.F.W. Bader, Atoms in molecules in external fields, J. Chem. Phys. 91 (1989) 6989–7001.
[67] R.F.W. Bader, Y. Tal, S.G. Anderson, T.T. Nguyen-Dang, Quantum topology: theory of molecular structure and its change, Isr. J. Chem. 19 (1980) 8–29.
[68] T.R.T. Koritsanszky, P. Macchi, C. Gatti, L.J. Farrugia, P.R. Mallinson, A. Volkov, A Computer Program Package for Multipole Refinement, Topological Analysis of Charge Densities and Evaluation of Intermolecular Energies from Experimental or Theoretical Structure Factors Manual Version September 2007 Program Version 5.42 September 2007 XD, Program, 2007.

[69] D.B. Kitchen, H. Decornez, J.R. Furr, J. Bajorath, Docking and scoring in virtual screening for drug discovery: methods and applications, Nat. Rev. Drug Discov. 3 (2004) 935–949.
[70] W. Sherman, H.S. Beard, R. Farid, Use of an induced fit receptor structure in virtual screening, Chem. Biol. Drug Des. 67 (2006) 83–84.
[71] R.A. Friesner, J.L. Banks, R.B. Murphy, T.A. Halgren, J.J. Klicic, D.T. Mainz, M.P. Repasky, E.H. Knoll, M. Shelley, J.K. Perry, D.E. Shaw, P. Francis, P.S. Shenkin, Glide : A New Approach for Rapid , Accurate Docking and Scoring . 1 . Method and Assessment of Docking Accuracy, 2004, pp. 1739–1749.
[72] R.A. Friesner, R.B. Murphy, M.P. Repasky, L.L. Frye, J.R. Greenwood, T.A. Halgren, P.C. Sanschagrin, D.T. Mainz, Extra precision glide: docking and scoring incorporating a model of hydrophobic enclosure for protein-ligand complexes, J. Med. Chem. 49 (2006) 6177–6196.
[73] N. Brooijmans, I.D. Kuntz, Molecular recognition and docking algorithms, Annu. Rev. Biophys. Biomol. Struct. 32 (2003) 335–373.
[74] W. Sherman, T. Day, M.P. Jacobson, R.A. Friesner, R. Farid, Novel Procedure for Modeling Ligand/Receptor Induced Fit Effects, 2006, pp. 534–553.
[75] A. Renuga Parameswari, G. Rajalakshmi, P. Kumaradhas, A combined molecular docking and charge density analysis is a new approach for medicinal research to understand drug-receptor interaction: curcumin-AChE model, Chem. Biol. Interact. 225 (2015) 21–31.
[76] P. Munshi, T.N. Guru Row, Intra- and intermolecular interactions in small bioactive molecules: cooperative features from experimental and theoretical charge-density analysis, Acta Crystallogr. Sect. B Struct. Sci. 62 (2006) 612–626.
[77] N. Dadda, A. Nassour, B. Guillot, N. Benali-Cherif, C. Jelsch, Charge-density analysis and electrostatic properties of 2-carboxy-4-methylanilinium chloride mono-hydrate obtained using a multipolar and a spherical-charges model, Acta Crystallogr. Sect. A Found. Crystallogr. 68 (2012) 452–463.
[78] H. Govindasamy, S. Magudeeswaran, K. Poomani, Identification of novel flavonoid inhibitor of Catechol-O-Methyltransferase enzyme by molecular screening, quantum mechanics/molecular mechanics and molecular dynamics simulations, J. Biomol. Struct. Dyn. (2019).
[79] M. Sivanandam, K. Saravanan, P. Kumaradhas, Insights into intermolecular interactions, electrostatic properties and the stability of C646 in the binding pocket of p300 histone acetyltransferase enzyme: a combined molecular dynamics and charge density study, J. Biomol. Struct. Dyn. 1102 (2017) 1–19.
[80] S. Dasgupta, S. Mukherjee, B.P. Mukhopadhyay, A. Banerjee, D.K. Mishra, Recognition dynamics of dopamine to human Monoamine oxidase B: role of Leu171/Gln206 and conserved water molecules in the active site cavity, J. Biomol. Struct. Dyn. 36 (2018) 1439–1462.
[81] M.Y. Lobanov, N.S. Bogatyreva, O.V. Galzitskaya, Radius of gyration as an indicator of protein structure compactness, Mol. Biol. 42 (2008) 623–628.
[82] K. Yelekçi, Ö. Karahan, M. Toprakçi, Docking of novel reversible monoamine oxidase-B inhibitors: efficient prediction of ligand binding sites and estimation of inhibitors thermodynamic properties, J. Neural. Transm. 114 (2007) 725–732.
[83] S. Magudeeswaran, K. Poomani, Binding mechanism of spinosine and venenatine molecules with p300 HAT enzyme: molecular screening, molecular dynamics and free-energy analysis, J. Cell. Biochem. (2019).
[84] D. Bonivento, E.M. Milczek, G.R. McDonald, C. Binda, A. Holt, D.E. Edmondson, A. Mattevi, Potentiation of ligand binding through cooperative effects in monoamine oxidase B, J. Biol. Chem. 285 (2010) 36849–36856.
[85] G. Felice, D. Alberga, L. Pisani, D. Gadaleta, D. Trisciuzzi, R. Farina, A. Carotti, G. Lattanzi, M. Catto, O. Nicolotti, European Journal of Pharmaceutical Sciences A rational approach to elucidate human monoamine oxidase molecular selectivity, Eur. J. Pharm. Sci. 101 (2017) 90–99.